Supplentary material for: Soliton gases and generalized hydrodynamics

Benjamin Doyon,[1] Takato Yoshimura,[1] and Jean-Sébastien Caux[2]

[1] *Department of Mathematics, King's College London, Strand, London WC2R 2LS, UK*
[2] *Institute for Theoretical Physics Amsterdam and Delta Institute for Theoretical Physics, University of Amsterdam, Science Park 904, 1098 XH Amsterdam, The Netherlands*

I. FLEA GAS ALGORITHM

The gas is represented by a chain of cells, each cell representing a quasi-particle A and containing all necessary information pertaining to it (its velocity, its type, its position A.pos on the line), ordered from left to right. The procedure distance(A, B) returns the oriented distance of the jump for a collision of A against B (it depends on the velocities and types of A and B); it was denoted $d(\cdot, \cdot)$ in the text, and it is positive for forward jumps, negative for backward jumps. In order not to perform a given jump, associated to a give crossing, twice, we need to mark the pairs of quasi-particle at their first collision; marked pairs, if they collide another time, just past through each other. This is of course essential if jumps are backwards, and in general has the effect that under the re-organization of quasi-particles' positions in a neighborhood of a collision, the exact distance $d(\cdot, \cdot)$ has been jumped by every quasi-particle affected by a collision. A picture for possible collisions between quasi-particles with velocities v and w are depicted in the Fig.1, and a precise algorithm for the flea gas is as follows.

```
procedure Evolve:
Displace all until next collision;
Collide left-particle against right-particle;
repeat until evolution time has elapsed;
end.

procedure Collide A against B:
if marked (A, B):
  Exchange A, B in the chain
else:
  Mark (A, B);
  Jump A by distance(A, B);
  Jump B by −distance(A, B);
end.

procedure Jump A by D:
if D < 0 then side is left;
else side is right;
repeat:
  B := quasi-particle to the side of A;
  if B exists and |A.pos − B.pos| < |D|:
    D := D − B.pos + A.pos;
    A.pos := B.pos;
    if side is left:  Collide B against A;
    else:  Collide A against B;
  else:
    A.pos := A.pos + D;
    break;
end.
```

Above, side refers to the side within the chain. Note that, because of the recursive process (the chain reaction of collisions), the event Jump A by distance(A, B) may also affect the position of B. This is fine, as long as B then jumps by the correct distance afterwards. Of course, the choice of making A jump before B in the Collide procedure is arbitrary. Different orderings lead to different microscopic re-organizations of quasi-particles' positions at collisions, but to the same large-scale Euler hydrodynamics.

An acceleration due to an external field is implicitly implemented with the Displace procedure. There, the evolution of each quasi-particle changes, in general, both its position and its velocity, as per the usual physical laws for particles within external force fields. With an acceleration potential, it is possible that pairs of particles that collided, and thus were marked, meet again after a macroscopic time (for instance in a harmonic potential). We thus need to "unmark" marked pairs after a mesocopic time: a time that is larger than that characteristics of the microscopic dynamics, but smaller than typical macroscopic times after which particles can meet again. There is thus a "forgetting time" that needs to be set, and that depends on the detail of the external potential.

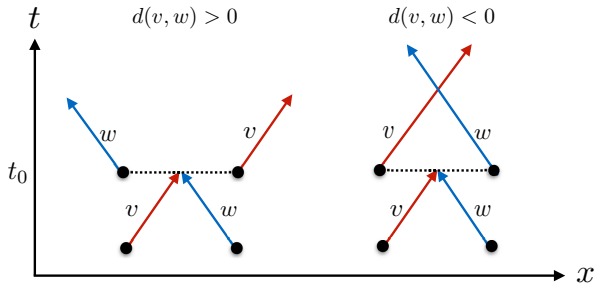

FIG. 1. A cartoon picture for collisions between quasi-particles with velocities v and w. Upon a collision at time t_0, they move forward or backward depending on the sign of $d(v, w)$.

Other algorithms are possible. In particular, it is not necessary to perform jumps "instantaneously" at collisions; as long as the distance $d(\cdot, \cdot)$ is added to the trajectory in a microscopic time, the large-scale effect is the same. For instance, one may associate to each quasi-particle a "ghost velocity change" Δv, used for time evolution in order to add an appropriate distance, but not

for the calculation of the jump distance (which uses the original spectral parameter and quasi-particle type). We choose an overall time $t_{\rm micro} > 0$. A quasi-particle either is in a "ghost" state ($\Delta v > 0$), or not ($\Delta v = 0$). We note the time t_0 of the start of a ghost state. Upon a collision of A with B, we do $\Delta v := \Delta v + \Delta t/\texttt{distance}(A, B)$, so that within a time Δt, the correct distance is added. When entering a ghost state (at a collision), we set $\Delta t = t_{\rm micro}$, while for further collisions during the ghost state, we choose $\Delta t = t_{\rm micro} - t + t_0$, where t is the time. The particle reverts to its normal state when $t - t_0 = t_{\rm micro}$.

II. THE LIEB-LINIGER MODEL IN THE ATTRACTIVE REGIME

In first-quantized form, the Lieb-Liniger (LL) model is described by the Hamiltonian

$$H = -\frac{1}{2m}\sum_{j=1}^{N}\frac{\partial^2}{\partial x_j^2} + c\sum_{j_1<j_2}\delta(x_{j_1} - x_{j_2}). \tag{1}$$

With repulsive interaction, $c > 0$, the spectrum of Bethe excitations is composed of a single particles, and the differential scattering phase given by (4) (main text). The case of attractive interaction $c = -2\bar{c} < 0$ is however not simply obtained by replacing c by $-2\bar{c}$ in (4) (main text). Instead, the spectrum of Bethe excitations is more complicated: it is composed of an infinity of Bethe strings, one for every positive length $j = 1, 2, 3, \ldots$. The attractive LL model is therefore classically implemented as a gas with infinitely-many species, representing the infinitely-many string lengths, all interacting with each other via a string-length- and velocity-dependent shift.

A thermodynamic Bethe ansatz analysis gives the following (we take $m = 1/2$ for simplicity). The energy and momentum functions, for a string of length a with "pseudo-momentum" λ, are given by

$$E(\lambda, j) = j\lambda^2 - \frac{\bar{c}^2}{12}j(j^2-1), \quad p(\lambda, j) = j\lambda. \tag{2}$$

The velocity is therefore

$$v^{\rm gr}(\lambda, j) = 2\lambda \tag{3}$$

which allows us to parametrize energy and momentum functions in terms of velocities,

$$E(\boldsymbol{v}) = \frac{jv^2}{2} - \frac{\bar{c}^2}{12}j(j^2-1), \quad p(\boldsymbol{v}) = \frac{jv}{2}. \tag{4}$$

The differential scattering phase, expressed in the pseudo-momentum coordinates λ, is the following function:

$$\begin{aligned}&\varphi((\lambda, j), (\lambda', j'))\\ &= (1-\delta_{j,j'})a_{|j-j'|}(\lambda-\lambda') + 2a_{|j-j'|+2}(\lambda-\lambda') + \ldots\\ &\quad \ldots + 2a_{j+j'-2}(\lambda-\lambda') + a_{j+j'}(\lambda-\lambda')\end{aligned} \tag{5}$$

where

$$a_j(\lambda) = \frac{j\bar{c}}{\lambda^2 + (j\bar{c}/2)^2}. \tag{6}$$

The above can be directly applied to the formulae presented in the main text, by taking pseudo-momenta λ as "rapidities" (this is a good definition as the differential scattering phase depends on differences of pseudo-momenta), and identifying gas species a with string lengths j.

III. MONOTONICITY OF THE EFFECTIVE VELOCITY

Here we provide a demonstration that, under certain conditions on the differential scattering phase, the effective velocity is monotonic with θ (this is a fact that is used in the derivation in the main text).

Consider the case of a single particle in the spectrum:

$$v^{\rm eff}(\theta) = v^{\rm gr}(\theta) + \int {\rm d}\alpha\, \tilde{\varphi}(\theta,\alpha)\,\rho_{\rm p}(\alpha)\,(v^{\rm eff}(\alpha) - v^{\rm eff}(\theta)). \tag{7}$$

where $\tilde{\varphi}(\theta,\alpha) = \frac{\varphi(\theta,\alpha)}{p'(\theta)}$. Assume first that $\tilde{\varphi}(\theta,\alpha)$ is positive (and also that $\rho_{\rm p}(\theta)$ is positive) and that its derivative has the following sign (with $' = {\rm d}/{\rm d}\theta$):

$$(\theta-\alpha)\tilde{\varphi}'(\theta,\alpha) \le 0 \tag{8}$$

Assume also that θ parametrizes the group velocity in a monotonic fashion, $(v^{\rm gr})'(\theta) > 0$. Taking a derivative, we find

$$\begin{aligned}(v^{\rm eff})'(\theta) &= (v^{\rm gr})'(\theta) +\\ &+ \int {\rm d}\alpha\,\tilde{\varphi}'(\theta,\alpha)\,\rho_{\rm p}(\alpha)\,(v^{\rm eff}(\alpha) - v^{\rm eff}(\theta)) -\\ &- (v^{\rm eff})'(\theta)\int {\rm d}\alpha\,\tilde{\varphi}(\theta,\alpha)\,\rho_{\rm p}(\alpha)\end{aligned} \tag{9}$$

and thus

$$\begin{aligned}&\left(1 + \int {\rm d}\alpha\,\tilde{\varphi}(\theta,\alpha)\,\rho_{\rm p}(\alpha)\right)(v^{\rm eff})'(\theta)\\ &\quad = (v^{\rm gr})'(\theta) + \int {\rm d}\alpha\,\tilde{\varphi}'(\theta,\alpha)\,\rho_{\rm p}(\alpha)\,(v^{\rm eff}(\alpha) - v^{\rm eff}(\theta))\end{aligned}$$

Thanks to (8), the right-hand side of the latter equation is positive if $(v^{\rm eff})'(\theta) \ge 0$ for all θ, and thus this latter condition is consistent with this integral equation. That is, if we assume that the solution is obtainable by recursion, starting with $(v^{\rm eff})'(\theta) = (v^{\rm gr})'(\theta)$, then the solution is monotonic. With decaying asymptotic for the particle density $\rho_{\rm p}(\alpha)$ it is easy to see that $v^{\rm eff}(\theta) \sim v^{\rm gr}(\theta)$ as $\theta \to \pm\infty$, and thus $v^{\rm eff}(\theta)$ covers full range of velocities.

All conditions, including (8), are satisfied in the Lieb-Liniger model and the sinh-Gordon model.

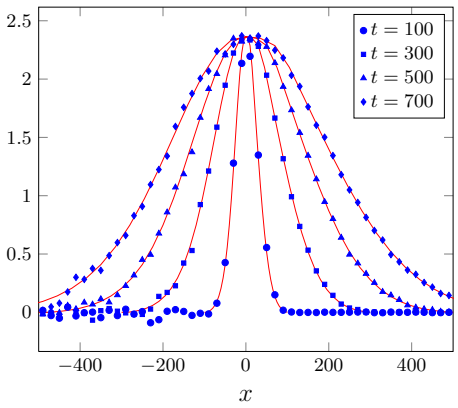

FIG. 2. GHD for the LL model with $m = 1$, $c = 1$ is simulated using the classical flea gas. Current profile from domain wall initial condition, initial left and right temperatures 10 and 1/3 (resp.), at times $t = 100$, 300, 500, 700. Simulation with approx. 2400 quasi-particles (initial baths of lengths 1000, open boundary condition) averaged over 1000 samples (blue); exact self-similar solution (red).

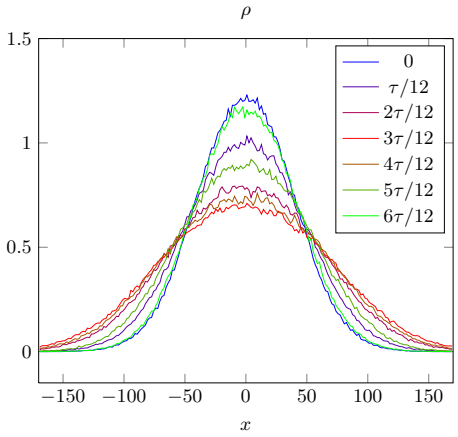

FIG. 3. Breathing motion of the LL model with $m = 1$, $c = 1$ occurring after change of frequency of a confining harmonic potential, simulated using the flea gas over half a period of the evolution potential. Colors go from blue (initial) to red (a quarter of a period) to green (half a period).

The condition on the sign of $\tilde{\varphi}(\theta, \alpha)$ may be relaxed, as long as

$$1 + \int \mathrm{d}\alpha \, \tilde{\varphi}(\theta, \alpha) \, \rho_{\mathrm{p}}(\alpha) > 0 \tag{10}$$

for all θ.

IV. ADDITIONAL NUMERICAL CHECKS

In the transport problem, in addition to the density, we have also verified numerically the accuracy of the current simulated by the classical flea gas as compared to the exact self-similar solution, in the Lieb-Liniger model. See Fig. 2. Again, the agreement is excellent, confirming the adequacy of the classical gas for representing GHD.

More interestingly, we have also simulated the "breathing motion" of the Lieb-Liniger model that is obtained after a change of the frequency of a harmonic potential. Consider adding a potential $V(x) = \omega_0^2 x^2/2$ to (1). The initial state is a thermal state within this potential, at temperature 1 (and throughout we keep $m = c = 1$). We then evolve this initial state within a wider potential, with $\omega = \omega_0/1.6$. The gas then expands and contracts in an almost periodic motion. The period is slightly larger than $\tau = 2\pi/\omega$ because of the interaction: particles are slowed down by the surrounding gas. See Fig 3 for an illustration of half a period (this is the case $L = 100$ described below, with a sampling of 4000).

In order to verify the accuracy of the GHD equations (3) (main text), we have numerically evaluated its integral version: the result of integrating the left-hand side over a phase-space-time cell $\mathcal{C} = X \times T \times \Theta$, as $\int_{\mathcal{C}} \mathrm{d}x \, \mathrm{d}t \, \mathrm{d}\theta \times$(l.h.s. of GHD equations). Further, in order to verify how the accuracy is related to the length scales of the hydrodynamic approximation, we have considered two situations, with two different overall variation scales L but with the same scattering length and the same range of interparticle distances.

We have chosen $L = 100$ and $L = 1000$. The initial particle density $\rho = \int \mathrm{d}\theta \rho_{\mathrm{cl}}(\theta)$ is supported mostly on $x \in [-L, L]$ and has a maximum 1.2 at the center $x = 0$. The central state at $x = 0$ is supported mostly on $\theta \in [-5, 5]$, and the evolution hamiltonian has period $\tau = 4L$. There are approximately $1.2L$ particles, and the "forgetting time" (see the description of the flea gas algorithm above) has been set to $\tau/10$. We have analyzed four types of cells: $|T| = L$ and $|T| = 3L$ (lengths of time of a quarter, and three quarter of a period), combined with $\Theta = \mathbb{R}$ and $\Theta = [-2, 2]$ (the full velocity space, and about half of the velocity support), in all cases choosing $|X| = L$. For $\Theta = \mathbb{R}$ we have looked at cells both around the center, $X = [-L/2, L/2]$, and nearer the boundary of the initial support, $X = [-4L/5, L/5]$, while for $\Theta = [-2, 2]$ we only consider the central cells. For each cell, we evaluated the relative error of the GHD equation, dividing by the total density and current on the boundaries of the cell (for simplicity we opted not to add the total force in the denominator):

$$E = \frac{\int_{X\times\Theta} \rho_{\mathrm{cl}}|_{\partial T} + \int_{T\times\Theta} (v^{\mathrm{eff}} \rho_{\mathrm{cl}})|_{\partial X} + \int_{X\times T} (-\partial_x V \, \rho_{\mathrm{cl}})|_{\partial\Theta}}{\int_{X\times\Theta} (\rho_{\mathrm{cl}}|_{T_+} + \rho_{\mathrm{cl}}|_{T_-}) + \int_{T\times\Theta} (|v^{\mathrm{eff}} \rho_{\mathrm{cl}}|_{X_+} + |v^{\mathrm{eff}} \rho_{\mathrm{cl}}|_{X_-})} \tag{11}$$

where $T_\pm$ and $X_\pm$ are the boundaries of $T = [T_-, T_+]$ and $X = [X_-, X_+]$, respectively. In all cases, we simulated the gas for a time $5\tau/4$ with $\Delta t = \tau/800$, and evaluated the average of E over all cells with T_- in the range from 0 up to $5\tau/4 - |T|$ (stepped by Δt). For finite-element approximations of integrals, we used this Δt, and $\Delta x = L/100$ and $\Delta\theta = 1/50$. The latter two also determine the sizes of fluid cells taken in order to evaluate densities.

We used a sampling of 1000 for $L = 100$, and 100 for $L = 1000$ (in the latter case each fluid cell contains 10 times as many particles as in the former case, hence less sampling is necessary).

The results are as follows:

$$
\begin{aligned}
X = [-L/2, L/2], |T| = L, \Theta = \mathbb{R} &: 0.21\%\ 0.10\% \\
X = [-L/2, L/2], |T| = 3L, \Theta = \mathbb{R} &: 0.60\%\ 0.10\% \\
X = [-4L/5, L/5], |T| = L, \Theta = \mathbb{R} &: 0.31\%\ 0.12\% \\
X = [-4L/5, L/5], |T| = 3L, \Theta = \mathbb{R} &: 0.90\%\ 0.16\% \\
X = [-L/2, L/2], |T| = L, \Theta = [-2, 2] &: 0.23\%\ 0.08\% \\
X = [-L/2, L/2], |T| = 3L, \Theta = [-2, 2] &: 0.66\%\ 0.08\%
\end{aligned}
$$

On the right-hand side, the first column of accuracies is for $L = 100$, the second is for $L = 1000$. The GHD equations are satisfied in all cases to quite high accuracy, showing that even for small numbers of particles, the hydrodynamic approximation is relatively accurate.

We note that the central cells probe regions of higher accuracy of the hydrodynamic approximation, as the particle density is higher and the actual variations of densities are lower. There are various trends in the accuracy, which are explainable as follows. (1) There is a large improvement from $L = 100$ to $L = 1000$, which is explained by the fact that as the variation length L is increased, all other lengths being the same, the hydrodynamic approximation is improved. (2) In the case $L = 100$, accuracy is lost by taking cells with longer time span $|T|$; presumably because the larger errors due to the slight breaking of the hydrodynamic approximation accumulate. In the case $L = 1000$, there is no such loss in accuracy for the central cells, which might suggest that the finite accuracy, in this case, is mainly due to the finite-element approximation. For the boundary cell, which probes regions where the hydrodynamic approximation is less accurate, there is such a loss, but it is not as pronounced as in the case $L = 100$. (3) Accuracy is lost from the central cell to the boundary cell, again due to the fact that the hydrodynamic approximation looses is accuracy.

Thus the trends of the results are fully in agreement with the general expectations from hydrodynamic, and confirm the validity of the flea gas algorithm within force fields.